

Contents lists available at ScienceDirect

Computers and Geosciences

journal homepage: www.elsevier.com/locate/cageo



Constraining uncertainty of fault orientation using a combinatorial algorithm

Michał Paweł Michalak^{a,b,1,*}, Ryszard Kuzak^{a,2}, Paweł Gladki^{c,3}, Agnieszka Kulawik^{d,4}, Yunfeng Ge^{e,5}

^a Institute of Earth Sciences, Faculty of Natural Sciences, University of Silesia in Katowice, Będzińska 60, 41-205, Sosnowiec, Poland

^b Faculty of Geology, Geophysics and Environmental Protection, AGH University of Science and Technology, Mickiewicza 30, 30-059, Cracow, Poland

^c Institute of Mathematics, Faculty of Science and Technology, University of Silesia in Katowice, Bankowa 14, 40-007, Katowice, Poland

^d Faculty of Science and Technology, University of Silesia in Katowice, Bankowa 14, 40-007, Katowice, Poland

^e Faculty of Engineering, China University of Geosciences, 388 Lumo Road, Wuhan, Hubei, China

ARTICLE INFO

Keywords:

Geological modeling

Fault evidence

Discontinuity orientation

Combinatorial algorithm

ABSTRACT

This study presents experimental results from assessing fault orientation using triangulation and a combinatorial algorithm. We constructed two geological surfaces with vertical and inclined faults. These surfaces were documented by boreholes and represented by triangulated surfaces. We first calculated orientations for a small sample of triangles genetically related to faults that were also members of the Delaunay triangulation. To reduce the epistemic uncertainty regarding the true fault strike, we applied a combinatorial algorithm that allowed us to investigate the orientation distribution of all planes genetically related to the fault. The experiment revealed three unintuitive effects that require further studies: 1) greater concentration of observations about the true dip direction; 2) the same dip direction for different triangles; and 3) triangles that dip in the opposite direction to the fault. To conduct spatial clustering within surfaces, we suggest considering a broader interval of orientations related to faults. This broader interval serves to honor the observation that orientations can be genetically related to faults, even if they indicate a relatively high directional within-dissimilarity. We suggest statistical methods for circular data to investigate the resulting distributions. The computer code associated with this study is open source and freely available.

1. Introduction

The characterization of fault networks within the subsurface is of great interest to structural geologists (Childs et al., 2009), geological engineers (Bandpey et al., 2019), geophysicists (Wu and Zhu, 2017), and even regional policy makers (Bond et al., 2007b). This is because fractures and faults control the spatial distribution and integrity of ore deposits, groundwater, or hydrocarbons. In subsurface geological modeling, uncertainties regarding fault topology, geometries, location, or existence may prevent the accomplishment of realistic geological

models (Bond, 2015; Schneeberger et al., 2017; Wellmann et al., 2010). This is primarily due to the limited quantity (Bruna et al., 2019) and quality (Godefroy et al., 2019; MacCormack et al., 2018) of available observations. Uncertainties are referred to as epistemic if they may be reduced if more knowledge or data are obtained. They are characterized as aleatory if the modeler sees no possibility of reducing them (Kiureghian and Ditlevsen, 2009). In quantitative structural geology, the reduction of epistemic uncertainties may be the case if more structural data are collected to characterize a fold (Bond, 2015).

Here, we reveal experimental results obtained by applying a

* Corresponding author. Faculty of Geology, Geophysics and Environmental Protection, AGH University of Science and Technology, Mickiewicza 30, 30-059, Cracow, Poland.

E-mail address: michalmichalak@us.edu.pl (M.P. Michalak).

¹ Michał Michalak devised the project, wrote the manuscript, performed the computations and discussed the results.

² Ryszard Kuzak discussed the limitations related to the geological applicability of the approach.

³ Paweł Gladki discussed the geometric problems of the proposed approach.

⁴ Agnieszka Kulawik calculated the required statistics.

⁵ Yunfeng Ge provided a broader discussion of the research context in the Introduction.

combinatorial algorithm (Lipski, 2004) to two faulted geological surfaces, represented by triangulated surfaces generated by Delaunay triangulation. The points (30 boreholes for each model with confirmed horizon depth) representing the surfaces come either from the hanging wall/footwall (vertical fault) or from the hanging wall/footwall/fault itself (non-horizontal fault). Both faults had their hanging wall lying to the west of the fault; however, the first fault was vertical and the second had a dip angle of 60°. The combinatorial algorithm generated all possible planes from an available set of points sampled throughout the faulted surfaces. The study design allowed for the rapid identification of triangles that were genetically related to the underlying faults. The expectations related to the employment of this combinatorial extension may be at first considered somewhat contradictory; however, they are offered as:

1. By using this extension, we aim to constrain the variability of the dip direction associated with the triangles cutting the fault. This indicates that having more observations characterizing a geological object may help reduce the epistemic uncertainty regarding its geometry (Bond, 2015; Kiureghian and Ditlevsen, 2009).
2. Because we will have more observations, we expect that new triangles can have orientations that do not necessarily lie within the initial range obtained through triangulation. This should entail greater directional variability among observations.

The first goal is of greater practical importance because the fault strike can be better constrained; for example, this can help achieve more accurate geological mapping. The latter goal is expected to provide a better understanding of the underlying methods and assessment of their realistic potential in subsurface modeling. Our study presents the inherent limitations of explicit approaches, but we also aim to provide insights into the extent to which the proposed approaches can complement implicit interpolation methods (Caumon et al., 2009; Collon et al., 2015; Wellmann et al., 2010) by combining the concepts of geological rules, graph theory, and combinatorics (compare Godefroy et al., 2021, 2019).

2. State of the art

2.1. Recognition of discontinuities in related fields

Indirect methods are often employed to characterize the discontinuities within the subsurface. This pertains particularly to a wide variety of methods related to Light Detection and Ranging (LiDAR) and photogrammetry (Seers and Hodgetts, 2016). These involve characterization of outcrop morphology, while discontinuities are recognized as traces cutting the outcrop face (e.g. Coubal et al., 2014). The relationship between the shape of the traces and outcrop morphology can serve to constrain the orientation of the underlying discontinuity (Seers and Hodgetts, 2016).

If the 3D points of the fault plane are available, then the orientation can be derived from the normal vector of the fitting plane to these selected points (Maerz et al., 2013). The manual method is a simple operation, however, it is time-consuming and its measurement accuracy highly depends on the subjective and skill level of geologists (compare Bond et al., 2007). On the other hand, several automatic or semi-automatic methods were developed to enhance the performance of discontinuity detection. In these methods, the difference in the normal vectors (Ge et al., 2018; Lato et al., 2009), curvature (Wang et al., 2017) or texture (Guo et al., 2019) of points (or facets) was often regarded as the criterion to cluster the points. Some statistical approaches and image segmentation algorithms were employed to identify the points located at the same discontinuity during the procedure of discontinuity detection, such as kernel density estimation (KDE) (Riquelme et al., 2014), clustering (Chen et al., 2016), principal component analysis (PCA) (Gomes et al., 2016) or region growing segmentation (Drews et al., 2018). After

discontinuity detection, the orientation of a discontinuity can be determined using the best-fitting plane approaches (Dewez et al., 2016; Gallo et al., 2018; Gigli and Casagli, 2011; Jones et al., 2016).

2.2. Spatial clustering

Discontinuities may also be recognized on Digital Elevation Models (DEM) or 3D models of rockmass. Rapid changes in orientation can serve for the expert-guided detection of potential discontinuities. For a DEM it is possible to incorporate edge-detection algorithms capable of detecting fractures and faults (Umili et al., 2013). For 3D models of rockmass (Lato et al., 2012; Riquelme et al., 2014) and DEMs (Brideau et al., 2012) special visualization techniques can be applied to exhibit the orientation patterns. They may, for example, involve color-coding specific subareas respective to their orientation (Brideau et al., 2012; Matasci et al., 2018; Riquelme et al., 2014) or adding colorful lights coming from directions corresponding to the normals to the discontinuities (Lato et al., 2012). The latter methods fall within the scope of more general objectives aiming to extract structural domains from orientation data with spatial aspect. The methods allowing to meet these objectives can be referred to as spatial clustering (Fisher, 1993). The basic version of such an approach involves the examination of two- or three-dimensional orientation data deprived of their spatial aspect. Having identified the reasonable number of geologically interpretable orientation patterns, it is then possible to combine the partitioning results with spatial information. From a technical viewpoint, this can be achieved through labeling the members of each cluster with a distinctive color or symbol (Fisher, 1993; Fisher et al., 1985, 1993) (Fig. 1). In this study, we propose a multi-stage methodology that is ultimately expected to offer a possibility for conducting spatial clustering for data collected throughout synthetic faulted geological surfaces documented by a network of boreholes.

2.3. Geometric trends in explicit approaches

Modeling geological structures often involves applying triangulation algorithms (Caumon et al., 2009; Ferrero et al., 2009; Michalak et al., 2019; Umili et al., 2013). Because the surfaces are represented explicitly, this kind of modelling is referred to as explicit (Collon et al., 2015). The three-point approach can be sometimes directly used to extract structural information (Allmendinger, 2020; Ferrero et al., 2009; Gonçalves et al., 2021; Michalak et al., 2019). For example (Michalak et al., 2019), proposed a new heuristic for determining the regional trend of a geological surface within the Kraków-Silesian Homocline in Poland. Retrieving information about the mean direction and slope of this surface was achieved through the following combinations of assumption and methods:

- This surface was assumed to be uniformly inclined in the north-eastern direction (Górecka, 2013; Marynowski et al., 2007; Woźniak et al., 2018; Woźniak and Bania, 2019; Znosko, 1960). However, small-scale changes associated with NE-SW faults did not allow simple averaging of orientations to be carried out.
- The resulting preferred orientation was extracted by averaging over the sub-population of similarly oriented triangles. For averaging, mean vector approach (Fisher, 1993) and inertia moment analysis (Davis, 2002; Fara and Scheidegger, 1961; Scheidegger, 1965a, 1965b; Watson, 1965, 1966) were used.
- The sub-population grouping genetically similar triangles was extracted by using Euclidean distance as a dissimilarity measure when performing cluster analysis.

However, at least two significant issues were not addressed (Michalak et al., 2019):

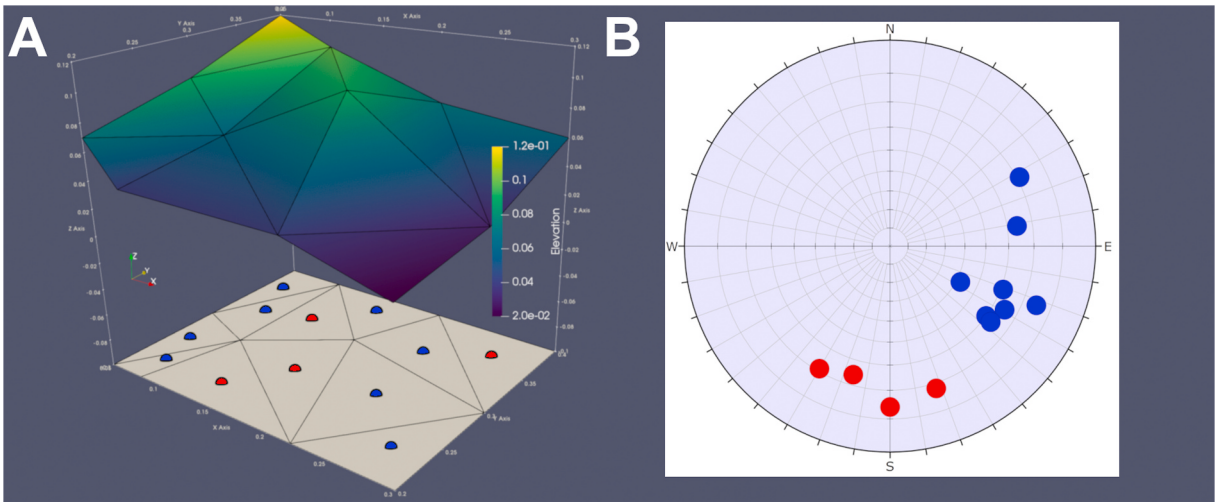


Fig. 1. The triangulation-based adaptation of spatial clustering method: (A) Colors corresponding to the assumed orientation trend are assigned to the geometric center of a flat triangle, which then allows for tracing orientation trends on a two-dimensional map; (B) Colors denote generalized geometrical information, as presented on the stereonet. The two clusters are separated in the vicinity of the azimuth of 145° . (For interpretation of the references to color in this figure legend, the reader is referred to the Web version of this article.)

1. The study was based on computing the orientation of a plane using three non-collinear points (i.e., the three-point method), but did not explain to what extent the three-point method is capable of retrieving the orientation of discontinuities that intersect the geological surface.
2. The extent to which orientation trends indicate spatial patterns was also not explained, a concept which naturally corresponds to the idea of spatial clustering (Fisher, 1993; Fisher et al., 1985, 1993).

3. Study design

3.1. Two faulted surfaces

To address potential and limitations underlying the two unsolved problems raised in section 2.3, we carried out numerical simulations for two geological surfaces documented by a network of boreholes. The workflow of the proposed methodology is presented on Fig. 2. For both faults, we used two different sets of 30 boreholes located within an elongated zone parallel to the fault strike (see Data Availability section to download the data sets). While both faults were striking N–S, they differed in their dip angle. The fault corresponding to the first surface was vertical, and the hanging wall was lying to the west of the fault (Fig. 3). From this it follows that the expected orientation of the model fault should be: $90^\circ \rightarrow 270^\circ$ (dip angle \rightarrow dip direction). The second case study involved a geological surface cut by a non-vertical fault (Fig. 4). Its dip angle was 60° , and its hanging wall was also lying to the west of the fault. Therefore, the expected orientation of the second fault model should be: $60^\circ \rightarrow 270^\circ$. To allow the reproducibility of results, mathematical descriptions of the case studies have been provided in Section 4.5 (see also Computer Code Availability for specific software). Computing the orientation of a plane based on three points (e.g. Groshong, 2006; Wellmann et al., 2016) was then applied to several cases that differed in the number of points involved in the simulation. For more than three-points involved in a case study, Delaunay triangulation was run. The orientations of the Delaunay triangles were then calculated and presented on the stereonets (Figs. 5–8).

3.2. Motivation for using the combinatorial algorithm

From the definition of triangulation it follows that for a given set of points a partition of the considered surface is established. From the structural viewpoint, in the triangulated model the number of

orientations is equal to the number of Delaunay triangles. Topologically, the generated orientations can be associated with the interiors of the Delaunay triangles, as their edges are shared by more than one triangle and cannot be associated with any orientation (Michalak et al., 2019). This partitional-in-nature method of sampling the orientation significantly reduces the number of available measurements. This may contribute to a greater uncertainty regarding the calculated orientation parameters (compare Pakyuz-Charrier et al., 2018).

Although bootstrap methods could be applied for reducing the uncertainty (Fisher, 1993), we suggest instead including new measurements in the analysis (see also Section 4.3 for a broader discussion of bootstrap methods). This inclusion can be achieved through employing a combinatorial algorithm for creating all three-element subsets from an n -element set. Equally, this algorithm serves to create all plausible planes from the given set of boreholes. As such, we are capable of investigating the orientation distribution of all triangles genetically related to a fault. This has the potential to better highlight the results of the conflict between reducing epistemic uncertainty and enriching the distribution with potentially more outlying observations.

4. Materials and methods

4.1. Outline of the three-point method

The computational framework allowing the orientation of a plane to be computed using three-point method is covered in geological textbooks (Groshong, 2006). To what extent the collinearity affects the reliability of orientation measurements is an open question; however, some heuristics regarding this case have been proposed (Collon et al., 2015; Michalak, 2018). These heuristics are based on a collinearity coefficient defined as the following ratio $\frac{l_1}{l_2+l_3}$, where $[l_1, l_2, l_3]$ is the sorted ($l_1 \geq l_2 \geq l_3$) vector of lengths associated with a 2-simplex (Michalak, 2018). The resulting ratio lies within the interval of $[0.5, 1]$ which follows from the triangle inequality and the fact that the lengths are sorted. Lower values are expected to point at equilateral triangles, while those approaching unity are assumed to represent collinear configurations. In the experimental research it was demonstrated that these collinear configurations may more often lie at the edge of the convex hull (Michalak et al., 2019). The nature of errors related to collinear configurations seems to be dual. They may relate to floating-point arithmetic round-off errors (Goldberg, 1991) and this in particular addresses configurations with collinearity coefficient dramatically close to one.

The synthetic case studies did not involve the incorporation of regional geological knowledge.

Fig.3E, Fig. 4A, 4B

Fig. 5, Fig. 6

Tab.1, Tab. 2

Algorithm 1. Computer Code Availability (3GeoCombine)

Tab. 5, Tab. 6

Fig. 9

Fig. 9

The synthetic case studies did not involve the incorporation of regional geological knowledge.

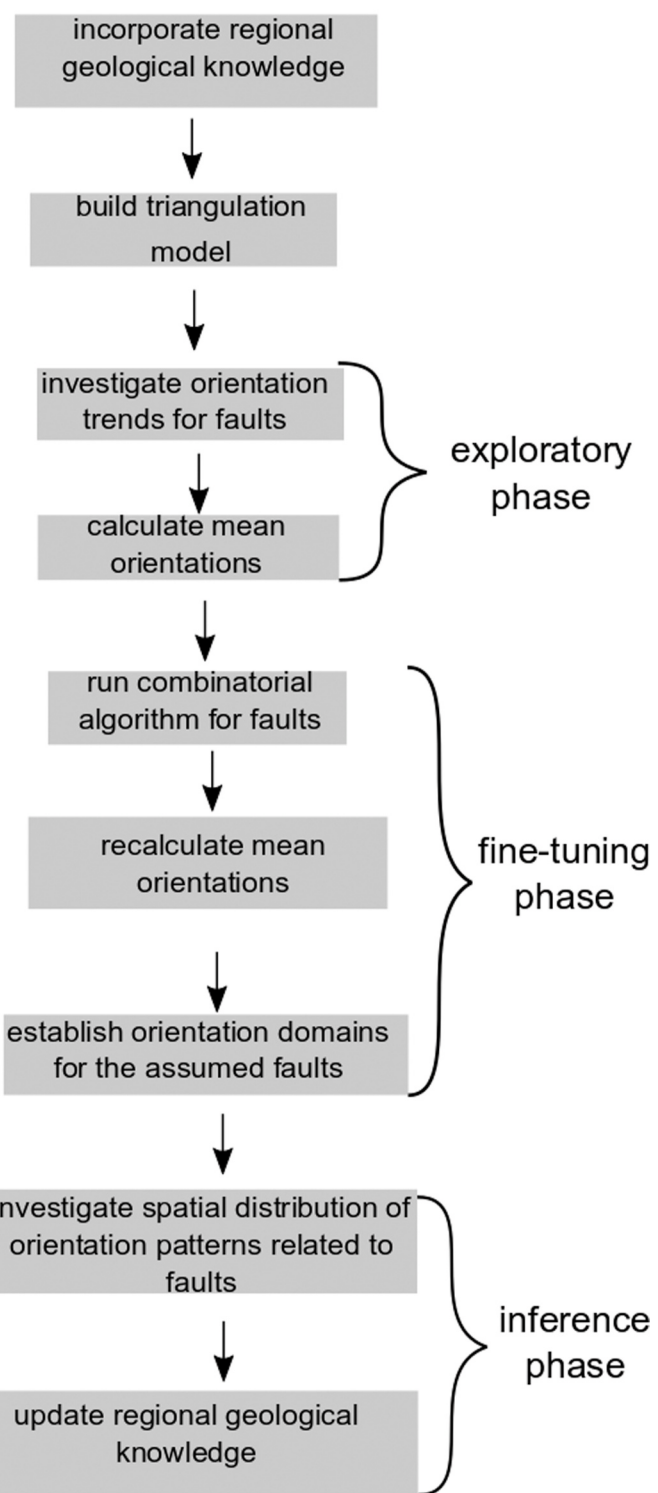


Fig. 2. Flowchart with steps performed in this study and corresponding resources.

But they may also be attributed to surface micro-roughnesses in which collinear configurations are trapped, being incapable of representing the general surface trend (Fig. 3).

4.2. Delaunay triangulation

From the viewpoint of graph theory, the definition of Delaunay triangulation states that it is a planar graph, being dual to the Voronoi diagram (De Berg et al., 2008).

Triangulation algorithms (implemented in CGAL (<https://www.cgal.org>)) (Boissonnat et al., 2002) allow the application of the three-point method at a larger scale, which is essential to obtain the population of orientation measurements. It is also crucial to the possibility of conducting spatial clustering throughout a faulted geological surface. The proposed version of this procedure assumes that the colors representing orientation domains are assigned to two dimensional Delaunay triangles. It is known that any triangulation of available points has $2n - 2 - k$ triangles, where n is the number of points and k is the number of

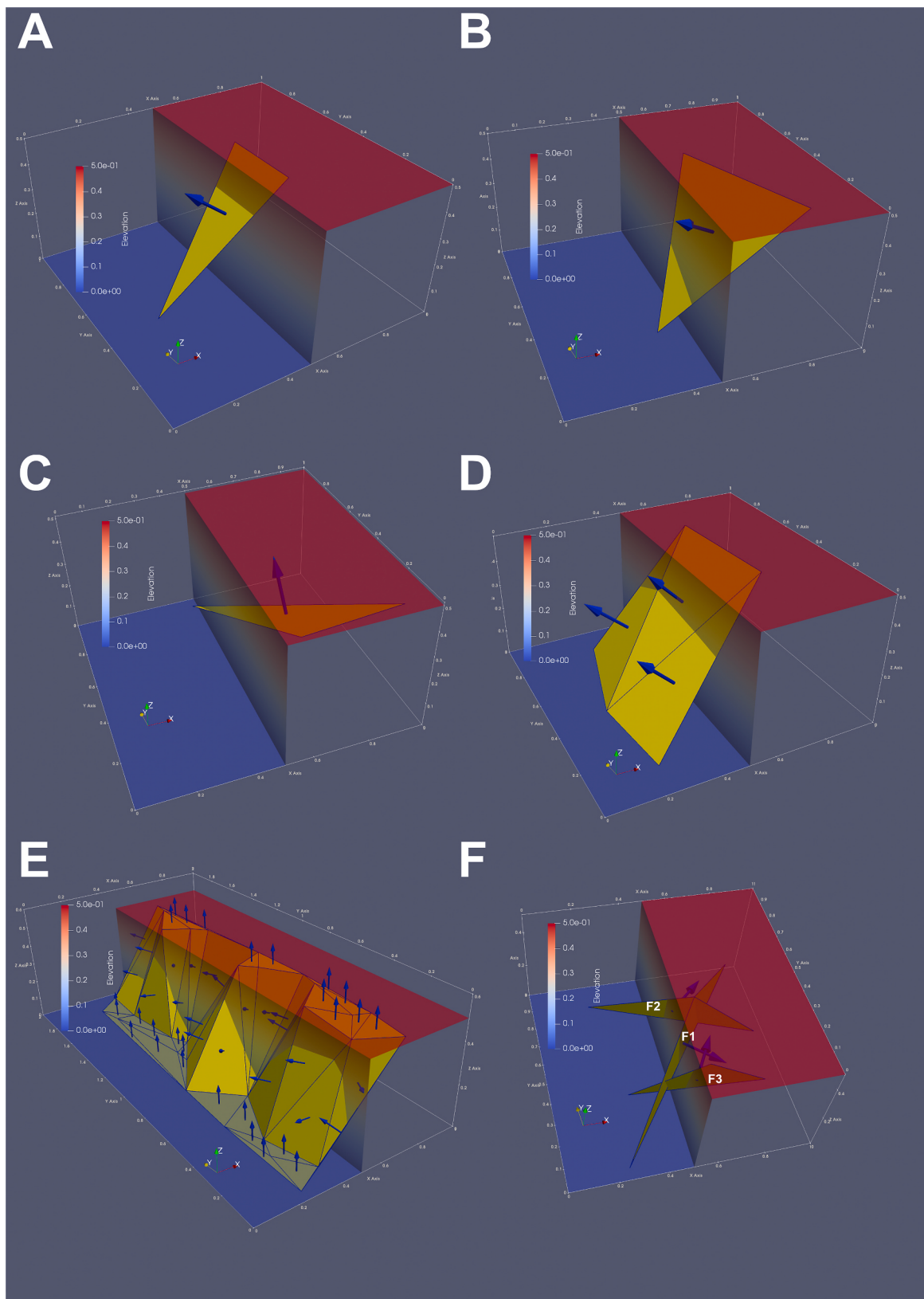


Fig. 3. Case study with a geological surface cut by a vertical fault: (A) the dip direction of the triangle considered is identical with the fault dip direction (270°); (B) the triangle is dipping to the SW; (C) the triangle is dipping to the N; (D) a triangulated model – all triangles are cutting the model fault surface; (E) an even greater triangulated model, generated using 30 boreholes located on hanging wall or footwall. Note several horizontal triangles whose all vertices lie either on the hanging wall or footwall; (F) unexpected dip directions of triangles taken from the set of all triangles that can be created from the set of points. Blue arrows are normal vectors to the triangles. (For interpretation of the references to color in this figure legend, the reader is referred to the Web version of this article.)

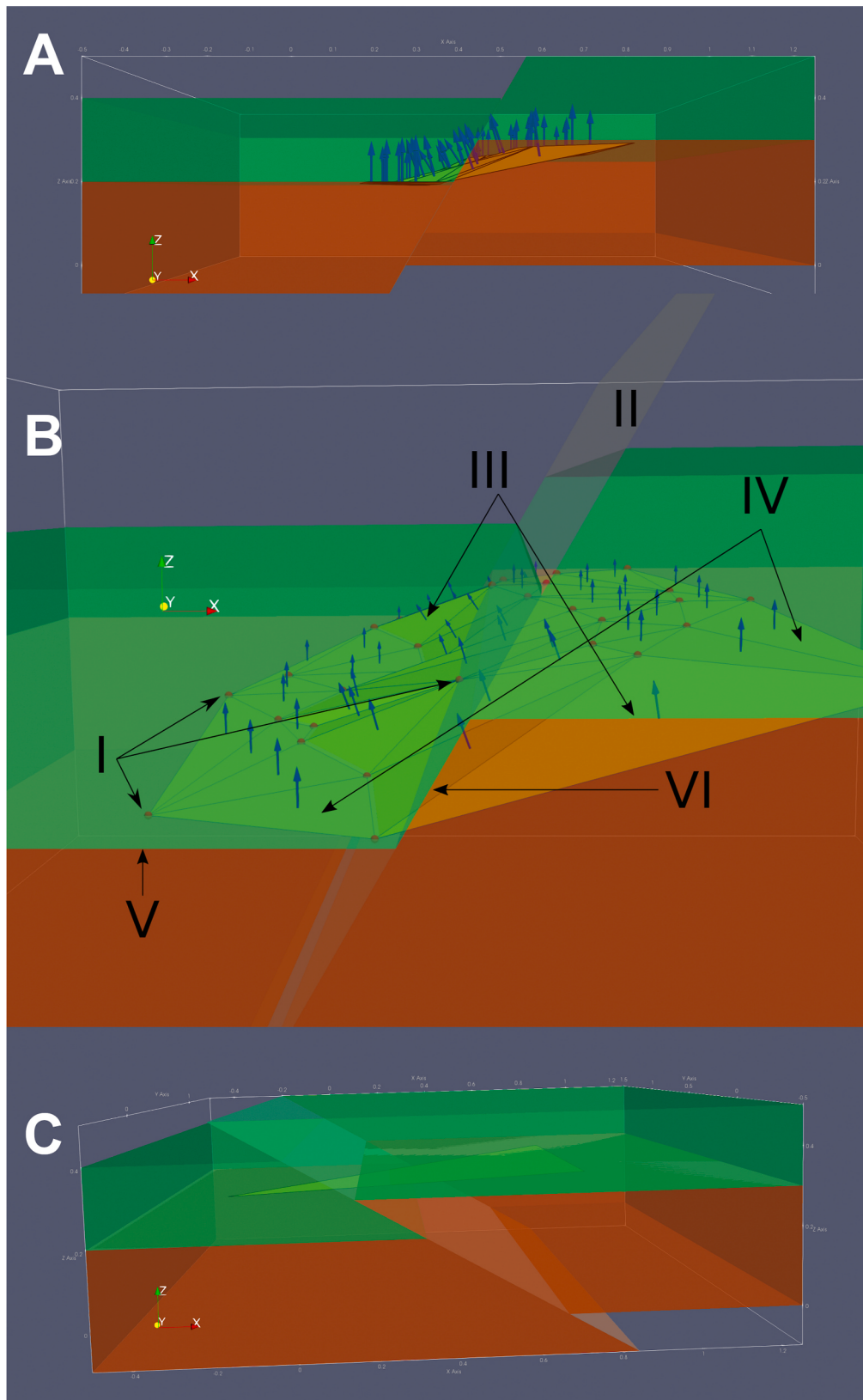


Fig. 4. Two non-vertical faults cutting a geological surface between green and orange unit: (A) normal fault with 60° of dip and dip direction of 270°: a view in the XY plane allows the geometry of the faulted surface to be better observed; (B) presentation of the terminology used: I (red points) – input points (boreholes), note that the borehole (marked by the middle arrow) with coordinates 0.42 (X ParaView axis) and 0.05 (Y ParaView axis) was located within the zone within which the fault acts as a contact, II – fault, III (inclined triangles) – triangles genetically related to fault, IV (horizontal triangles) – triangles genetically unrelated to fault, V – a stratigraphic contact (according to (Thiele et al., 2016)), VI – a faulted contact (according to (Thiele et al., 2016)); (C) a triangle cutting an inverse fault dipping at 30° to the east. This illustrates that the proposed method is not capable of calculating the fault dip direction but only its strike. (For interpretation of the references to color in this figure legend, the reader is referred to the Web version of this article.)

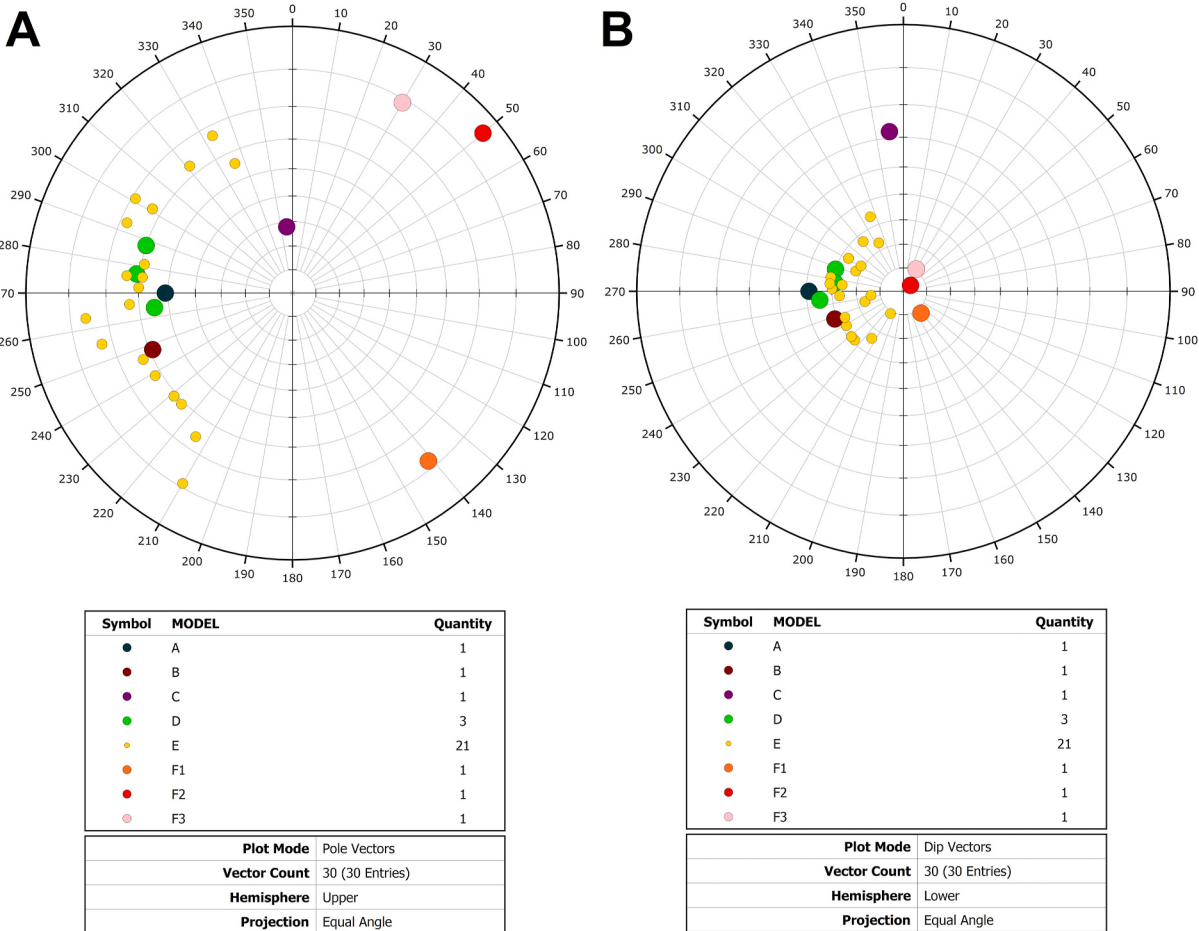


Fig. 5. Orientation of triangles taken from the case-studies with geological surface cut by a vertical fault: (A) pole vector mode; (B) dip vector mode. It seems that due to significant steepness of orientation measurements the pole vector mode serves to better enhance the variability of dip direction. The models A-F correspond to those presented on Fig. 3.

points that lie on the boundary of the convex hull. However, it is important to note that not all planes from the total of $2n - 2 - k$ should be included in the stereographic projection. This is because in our model, the triangles that are more external to the fault surface indicate horizontal orientation (Fig. 4B).

4.3. Algorithm for creating all three-element subsets

The partitional nature of triangulation entails substantial restriction to the number of observations that can be taken for modeling the fault geometry. It is reasonable to assume that in practice the number of observations (triangles) available in a faulted zone will not exceed two dozen. This suggests using bootstrap methods for calculating the mean direction and confidence intervals. Bootstrap methods are recommended if only a small amount of observations (less than 25) are available. The bootstrap procedure requires calculating the distribution of the sample mean \bar{X} by repeated re-sampling from the data. The main drawback of this method is the assumption that the data themselves are the true underlying distribution (Fisher, 1993). This may not always be the case, as the smaller sample may not be representative. Our idea to overcome this issue is to create new planar measurements from among all pointwise observations (boreholes). To achieve this, we employed a combinatorial algorithm (Lipski, 2004) for creating all three-element subsets from the given set of n points. Geologically speaking, this algorithm produced all triangles that can be created from boreholes within a reasonable neighborhood of the fault. The number of generated planes with respect to the number of available points is given in Table 1.

Algorithm 1. (for creating all k -element subsets from an n -element set).

Algorithm 1 (for creating all k -element subsets from an n -element set).

Input data: n, k

Expected results: sequence of all k -element subsets of the set $\{1, \dots, n\}$

begin

for $i := 1$ **to** k **do** $A[i] := i$; (*the first subset*)

$p := k$;

while $p \geq 1$ **do**

begin *write* ($A[1], \dots, A[k]$);

if $A[k] = n$ *then* $p := p - 1$ *else* $p := k$;

if $p \geq 1$ *then*

for $i := k$ **downto** p **do** $A[i] := A[p] + i - p + 1$

end

end

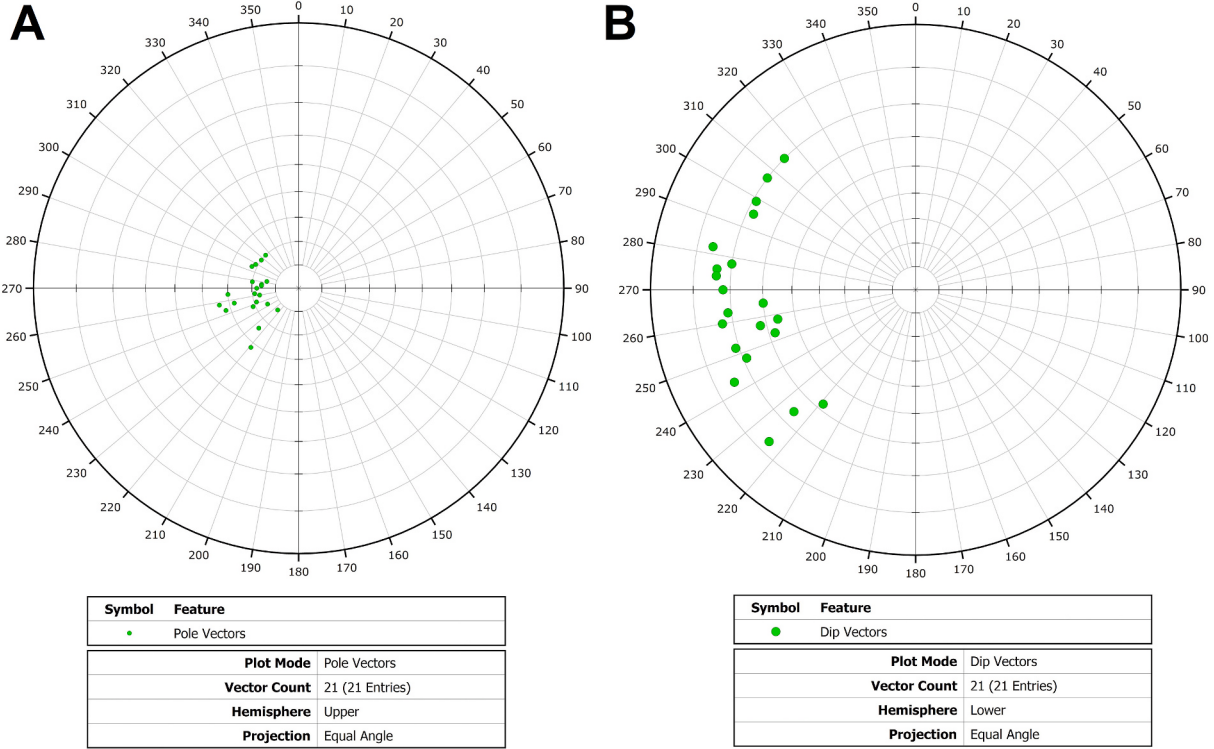


Fig. 6. Orientation of the triangles taken from the case study with a geological surface cut by a non-vertical fault (Fig. 4A and B): (A) pole vector mode; (B) dip vector mode. It can be seen that the dip vector mode serves to better enhance the variability of dip direction.

It must be realized, however, that the above algorithm produces only sequences of numbers and it is not capable itself of generating planes. Therefore, incorporating this algorithm into our case required the produced sequences of numbers to be regarded as indices of the array of 3D points. An open-source and freely available computer code can be downloaded from the GitHub repository (see Computer Code Availability for details).

4.4. Statistical analysis

4.4.1. Two-dimensional approach

In this approach, three-dimensional normal vectors to Delaunay triangles were first projected onto the horizontal plane. The essential changes introduced by this projection were that the Z – coordinates of the projected vectors were zero, but to obtain the unit length of the projected vectors, the X and Y coordinates of these vectors were divided by their length.

As a result, we used two-dimensional representations of the projected vectors that maintain the direction of the dip related to the original normal vectors. The averaging of orientation measurements was carried out using circular mean. Obtaining the mean vector requires the following values to be calculated (Fisher, 1993; Mardia and Jupp, 2008):

$$\bar{C} = \frac{1}{n} \sum_{i=1}^n \cos \theta_i, \quad \bar{S} = \frac{1}{n} \sum_{i=1}^n \sin \theta_i, \quad \text{where } \theta_i \text{ denotes the direction of the projected three-dimensional normal vector to Delaunay triangle } i \text{ onto the horizontal plane.}$$

The mean direction of the directions $\theta_1, \dots, \theta_n$ is denoted by $\bar{\theta}$ and is calculated as follows (Equation (1)):

$$\bar{\theta} = \begin{cases} \tan^{-1}\left(\bar{S}/\bar{C}\right), & \bar{S} > 0, \bar{C} > 0 \\ \tan^{-1}\left(\bar{S}/\bar{C}\right) + \pi, & \bar{C} < 0 \\ \tan^{-1}\left(\bar{S}/\bar{C}\right) + 2\pi, & \bar{S} < 0, \bar{C} > 0 \end{cases} \quad (1)$$

We calculated also the sample median direction $\tilde{\theta}$ of angles $\theta_1, \dots, \theta_n$ and it is any angle φ such that (i) half of the data points lie in the arc $[\varphi, \varphi + \pi]$ and (ii) the majority of the data points are nearer to φ than to $\varphi + \pi$ (Mardia and Jupp, 2008). Other summary statistics were also calculated: mean resultant length $\bar{R} = \sqrt{(\bar{C}^2 + \bar{S}^2)}$, circular standard deviation $v = \sqrt{-2\log \bar{R}}$, sample circular dispersion $\hat{\delta} = \frac{1-\bar{R}_2}{2\bar{R}^2}$, where $\bar{R}_2 = \frac{1}{n} \sum_{i=1}^n \cos 2(\theta_i - \bar{\theta})$ denotes the pth sample trigonometric moment (with $p = 2$) about the mean direction, and circular standard error $\hat{\sigma} = \sqrt{\frac{\hat{\delta}}{n}}$. We estimated also the 95% confidence intervals for the mean direction (Table 6). In triangulation-based models we used the procedure for the von Mises distribution because statistical tests did not disprove the hypothesis that the data were drawn from this distribution. However, this hypothesis was rejected for the combinatorial models, so we used non-parametric methods for large samples (Fisher, 1993).

4.4.2. Three-dimensional approach

The second method can be regarded as a multi-step optimization problem and it was developed by (Watson, 1966). A rewritten yet equivalent version of the method was described by (Davis, 2002). The geometric ideas behind this method can be summarized in the following points:

- 1) Orientation measurements are regarded as points lying on the unit sphere (or tips of corresponding unit vectors).
- 2) The mean orientation u is associated with a unit vector that minimizes the sum of squared distances between the vectors' end points (points lying on the unit sphere) to the line containing u .
- 3) Using Pythagorean theorem it can be shown that the sum of all distances to u can be expressed as $n - u^T A u$, where n is the number of observations and the matrix A in the quadratic form $u^T A u$ is real and symmetric (the definition is given in Equation (2)). The optimization

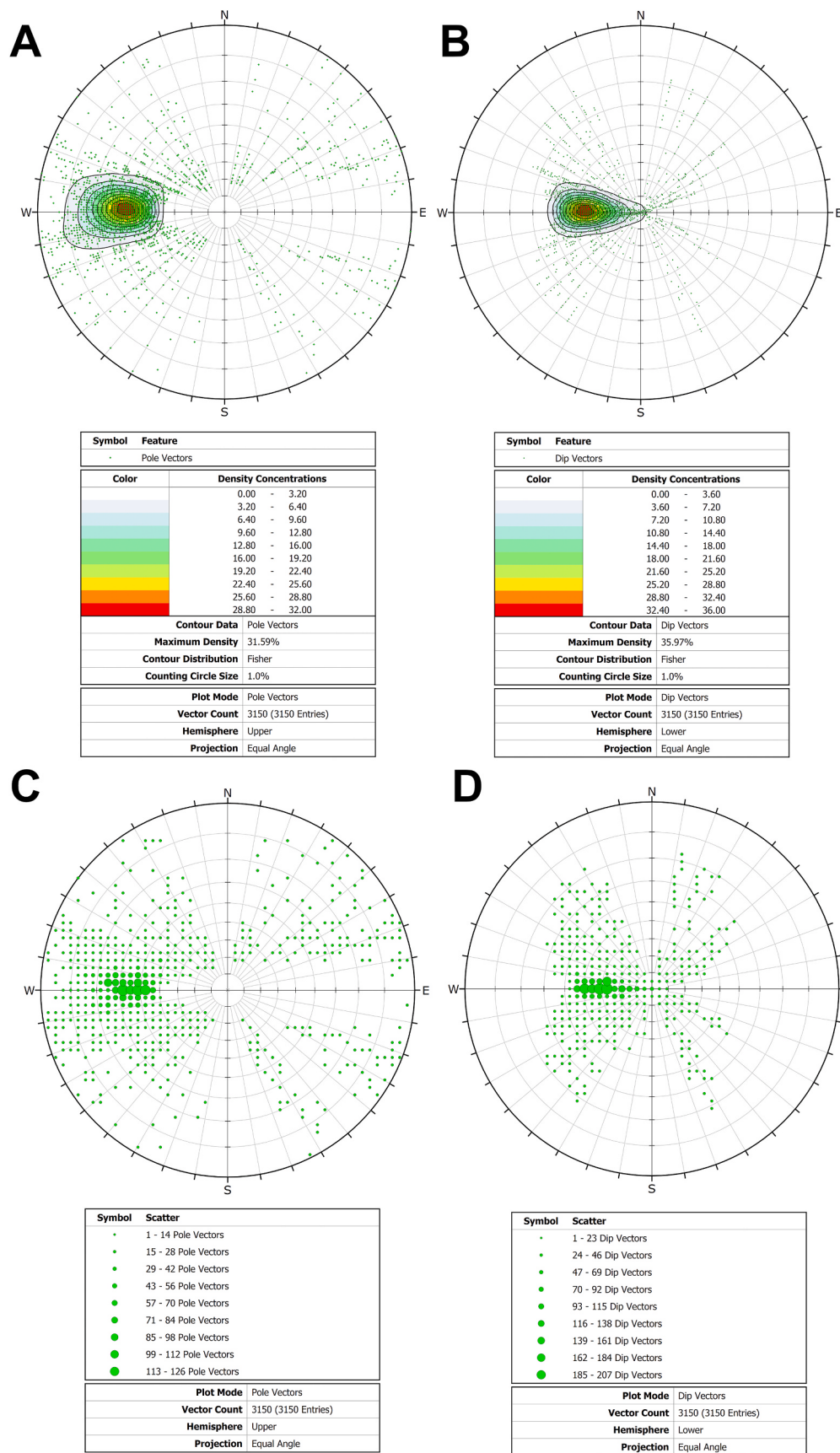


Fig. 7. Combinatorial algorithm that created all possible triangles from the model with vertical fault (Fig. 3E). Orientations of all triangles are presented on stereonets: (A) all measurements plotted in pole vector mode; (B) all measurements plotted in dip vector mode; (C) scatterplot in pole vector mode; (D) scatterplot in dip vector mode. It seems that due to significant steepness of orientation measurements the pole vector mode serves to better enhance the variability of dip direction. The dip vector mode, on the other hand, offers perhaps a greater concentration of measurements as for the expected dip direction.

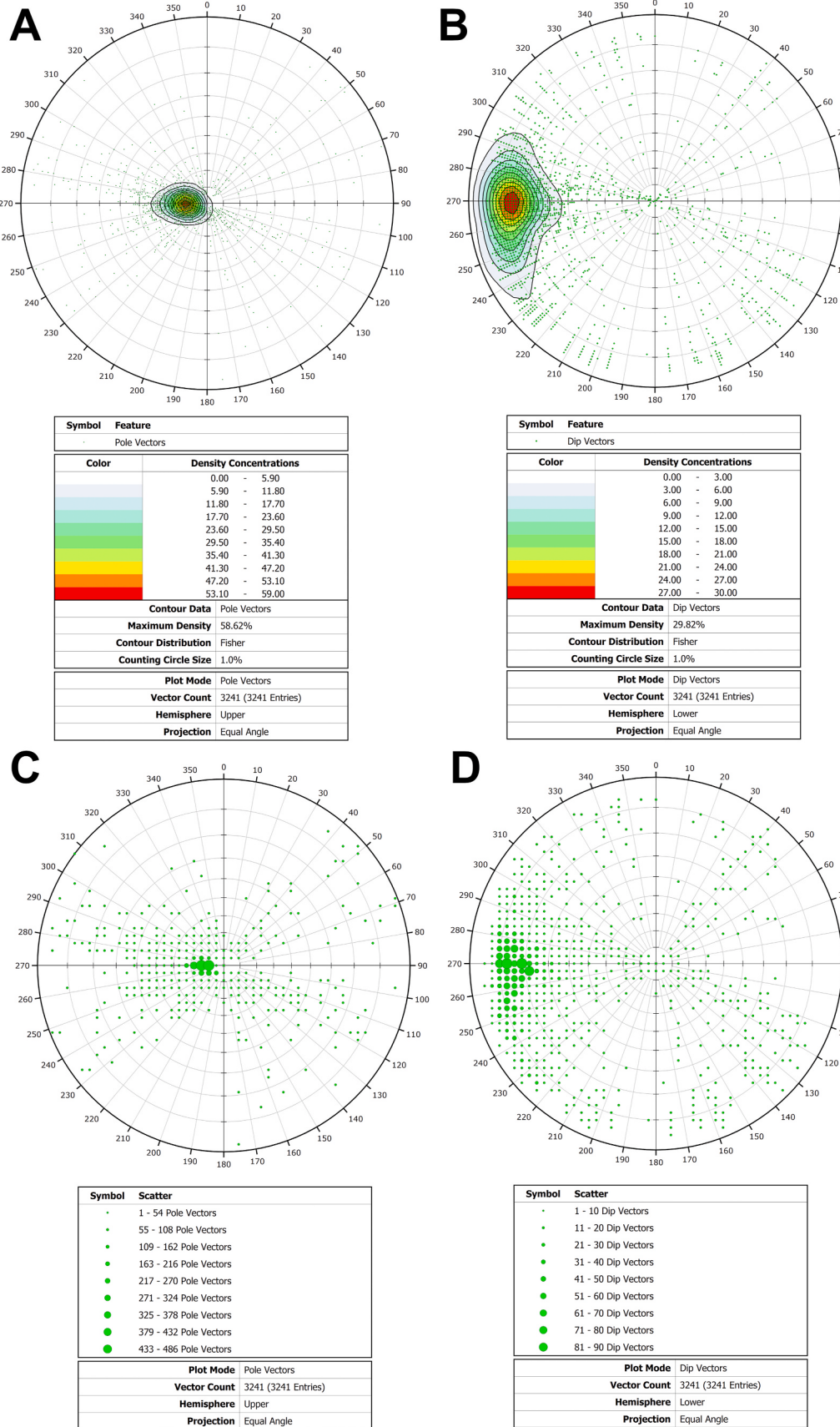


Fig. 8. Combinatorial algorithm that created all possible triangles from the triangulated model (Fig. 4A and B). Orientations of all triangles are presented on stereonets: (A) all measurements plotted in pole vector mode; (B) all measurements plotted in dip vector mode; (C) scatterplot in pole vector mode; (D) scatterplot in dip vector mode. It seems that due to subhorizontal orientation of measurements the dip vector mode serves to better enhance the variability of dip direction. The pole vector mode, on the other hand, offers perhaps a greater concentration of measurements as for the expected dip direction.

Table 1

Number of generated planes with respect to the number of available points. $C(n,k)$ denotes the binomial coefficient.

| n | 3 | 5 | 10 | 15 | 20 | 30 | 50 | 100 | 150 |
|-----------------------|---|----|-----|-----|------|------|-------|--------|--------|
| $C(n,k)$ with $k = 3$ | 1 | 10 | 120 | 455 | 1140 | 4060 | 19600 | 161700 | 551300 |

task is about finding u that minimizes $n - u^T A u$ (or equivalently finding u that maximizes $u^T A u$).

- 4) From applying eigendecomposition theory to real and symmetric matrices it can be shown that to find u that maximizes the quadratic form $u^T A u$ it is necessary to find the eigenvector belonging to the greatest eigenvalue of A .

$$A = \frac{1}{n} \begin{bmatrix} \Sigma a_i^2 & \Sigma a_i b_i & \Sigma a_i c_i \\ \Sigma b_i a_i & \Sigma b_i^2 & \Sigma b_i c_i \\ \Sigma c_i a_i & \Sigma c_i b_i & \Sigma c_i^2 \end{bmatrix}, \quad (2)$$

In Eq. (2), a_i, b_i, c_i correspond to the Cartesian coordinates XYZ of the normalized normal vectors, respectively, with n being the number of orientations. Computing the eigenvectors, v_1, v_2, v_3 , and corresponding eigenvalues, $\lambda_1, \lambda_2, \lambda_3$ is straightforward using the *eigen* function in R. In general, the eigenvalues can be normalized using $S_i = \lambda_i / n$, such that $S_1 + S_2 + S_3 = 1$. To characterize the resulting distribution two coefficients are suggested. While the first ratio $C = \ln(S_1/S_3)$ assesses the strength of the preferred orientation, the second $K = \ln(S_1/S_2)/\ln(S_2/S_3)$, appraises the shape of the observations' distribution. Low variability of orientation ($K > 1$) is typical for *clusters*, but if the distribution indicates greater directional variability ($0 < K < 1$) one can say about *girdles* (Woodcock, 1977).

4.5. Mathematical description of faulted surfaces

Both case studies required intersection of faults with geological surfaces. The mathematical description of the models corresponding to both vertical and inclined faults can be given within the context of linear algebra. In both versions, the hanging wall and footwall have horizontal position which corresponds to the unit normal vector $[0, 0, 1]$. This position is true for $x \in [0, 0.5] \cup (0.5, 1]$ and $x \in [-0.5, 0.388675] \cup (0.44641, 1.25]$ for vertical and inclined model, respectively. The fault orientations $90^\circ \rightarrow 270^\circ$ and $60^\circ \rightarrow 270^\circ$ correspond to unit normal vectors $[0, -1, 0]$ and $[0, 0.866025, 0.5]$, respectively, and can be assigned to complementary x-intervals described above.

As can be seen in Fig. 3, it is impossible for the vertical fault plane to be a separator between geological units (points are lying either on the hanging wall or footwall). This is, however, possible for the inclined fault that itself separates geological units within the narrow zone (e.g., Fig. 4). The width of this zone is naturally related to the fault dip angle.

For both case studies the following property is true:

Property 1. (property of the models).

A triangle is not horizontal if and only if not all of the three vertices lie on the same side of the fault.

We offer also a definition for triangles that are subject to the orientation data analysis (Definition 1).

Definition 1. (triangles genetically related to fault in the model).

A triangle is referred to as genetically related to fault if it is not horizontal.

5. Results

5.1. Synthetic case studies

For the vertical fault model, the dip angle of the triangles cutting the vertical fault were significantly smaller than that of the model fault dip (Fig. 3). It should not be assumed, however, that using this approach we can get a lower bound on the fault dip. This is because in the model with

fault dip of 60° , some triangles with a dip greater than 60° were generated (Table 2).

Another observation is that the dip direction of a triangle was found to vary within the range of at least 180° (Figs. 5 and 6). It was also observed that the observations related to triangulated models (Figs. 3E, 4A and 4B) often had dip directions similar to that of the expected dip direction (i.e., $\sim 270^\circ$), however, the small amount of observations generated through triangulation did not allow for a strong concentration of the results to be observed.

Having employed the combinatorial algorithm to all boreholes corresponding to Figs. 3E, 4A and 4B, it was possible to obtain more triangles whose orientation indicated greater concentration around the expected dip direction (Figs. 7 and 8). However, we also observed geometric singularities because dip directions from the “eastern” range (i.e., dip direction lying between 0 and 180°) were also present (Fig. 3F, objects F1–F3; Figs. 7 and 8). The calculated orientations of these singularities are provided in Tables 2 and 3.

The mean directions for the unfiltered (including more collinear) observations for the vertical fault varied from 268.89 to 272.29 , and for the fault inclined at 60° from 263.37 to 266.61 (Tables 4 and 5). Yet, to conducting spatial clustering of interest, not only the mean directions but also the typical variability of observations is required. We assumed that the results generated by the combinatorial algorithm would be more useful for assessing a reasonable directional variability intervals for triangles genetically related to fault. However, the presence of geometric outliers caused a significant inconvenience in accomplishing this. The observations lying in the eastern part of the stereonet constituted 7.75% and 8.08% of the output produced by the combinatorial algorithm for the vertical and inclined models, respectively. In both cases narrow zones of dip directions $[170^\circ, 190^\circ]$ and $[350^\circ, 10^\circ]$ were observed that were not densely covered with observations. Thus, one could argue that observations lying within the range of $[0^\circ, 180^\circ]$ could be regarded as outliers, and in this approach taking only “west-dipping” observations yields an approximately 92% directional variability interval. For the vertical fault, the left and right extremities would be 192° and 337° , while for the fault inclined at 60° , the corresponding values would be 183° and 355° , respectively. This method of determining the directional variability interval is relatively simple; however, one disadvantage is that it is sensitive to the outlying observations occurring in the western part of the stereonet. One way to mitigate this effect would be to symmetrically remove observations from the extreme parts of the reduced distribution. For example, for the inclined fault model one could get a 90% directional variability interval $[202^\circ, 332^\circ]$ through further reduction of observations. For the vertical fault model, it is also possible to get approximately 90% directional variability interval by establishing the left (by removing 32 “southern” observations) and right (by removing 34 “northern” observations) extremities to 225° and 328° , respectively. We note that it may be difficult to reduce the distribution in a perfectly symmetrical manner (i.e., by subtracting the same amount of observations from each side). This follows from the fact that many observations have the same dip direction (Tables 2 and 3) which can make it difficult to conduct the reduction through the removal of single observations.

5.2. Maps for conducting spatial clustering

With the geometrical centers of the Delaunay triangles (X_C, Y_C), it is straightforward to plot a map with colorful points assigned to these centers (Fig. 9). The colors represent specific orientation domains, according to the partition established either by clustering algorithms or by

Table 2

Sample results of all combinations created from the points considered in vertical case (E). Full table can be downloaded as a separate file. Some coordinates are double-denoted (by X_p and Y_p) which corresponds to a different coordinate system in ParaView. X_C, ..., Z_C denote the geometric centers of Delaunay triangles to which normal vectors (X_N, ..., Z_N) of these triangles were assigned.

| X _C (Y _p) | Y _C (X _p) | Z _C | X _N (Y _p) | Y _N (X _p) | Z _N | Dip_ang | Dip_dir | DOC | Model |
|--|----------------------------------|----------------|----------------------------------|----------------------------------|----------------|---------|---------|------|-------|
| 0.363 | 0.520 | 0.333 | -0.755 | 0.622 | 0.206 | 78.10 | 140.53 | 0.94 | F1 |
| 0.527 | 0.520 | 0.333 | 0.646 | 0.760 | 0.069 | 86.03 | 49.64 | 0.95 | F2 |
| 0.187 | 0.523 | 0.333 | 0.847 | 0.498 | 0.187 | 79.21 | 30.47 | 0.91 | F3 |
| | | | | | | | | | |
| Below different configurations with the same dip directions are given. They were not presented in the model, and are included only in the full version of the table. | | | | | | | | | |
| 0.387 | 0.500 | 0.333 | -0.772 | 0.635 | 0.026 | 88.49 | 140.53 | 0.95 | Table |
| 0.243 | 0.497 | 0.333 | 0.800 | 0.470 | 0.373 | 68.07 | 30.47 | 0.94 | Table |
| 0.243 | 0.497 | 0.333 | 0.800 | 0.470 | 0.373 | 68.07 | 30.47 | 0.94 | Table |

Table 3

Sample results of all combinations created from the points considered in the 60° dipping fault model. Full table can be downloaded as a separate file. Some coordinates are double-denoted (by X_p and Y_p) which corresponds to a different coordinate system in ParaView. X_C, ..., Z_C denote the geometric centers of Delaunay triangles to which normal vectors (X_N, ..., Z_N) of these triangles were assigned.

| X _C (Y _p) | Y _C (X _p) | Z _C | X _N (Y _p) | Y _N (X _p) | Z _N | Dip_ang | Dip_dir | DOC | Model |
|----------------------------------|----------------------------------|----------------|----------------------------------|----------------------------------|----------------|---------|---------|------|-------|
| 0.363 | 0.307 | 0.233 | -0.940 | 0.251 | 0.232 | 76.59 | 165.07 | 0.99 | Table |
| 0.463 | 0.557 | 0.267 | 0.775 | -0.415 | 0.476 | 61.57 | 331.82 | 0.99 | Table |
| 0.517 | 0.320 | 0.233 | 0.705 | -0.705 | 0.071 | 85.96 | 315.00 | 0.98 | Table |
| 0.540 | 0.267 | 0.233 | -0.168 | 0.045 | 0.985 | 10.00 | 165.07 | 0.93 | Table |
| 0.533 | 0.590 | 0.267 | 0.407 | -0.218 | 0.887 | 27.51 | 331.82 | 0.88 | Table |
| 0.300 | 0.290 | 0.218 | 0.094 | -0.094 | 0.991 | 7.67 | 315.00 | 0.67 | Table |

Table 4

Results from computing the orientation for the vertical (E) model: with triangulation and using a combinatorial model that created all possible planes.

| | |
|---------------------------------|-------------------------------|
| Observations from triangulation | Number of observations |
| | 21 |
| Circular mean | Dip Direction |
| | 269.62 |
| Combinatorial model | Number of observations |
| | 3150 |
| Circular mean | Dip Direction |
| | 272.75 |
| Observations from triangulation | Number of observations |
| | 21 |
| Inertia moment analysis | Orientation matrix |
| | Dip direction |
| | S ₁ 268.89 |
| | S ₂ 0.73 |
| | S ₃ 96.39 |
| | Dip angle |
| | 60.43 |
| | 86.77 |
| | 29.78 |
| | Eigenvalue |
| | 0.73169 |
| | 0.25339 |
| | 0.01492 |
| Combinatorial model | Number of observations |
| | 3150 |
| Inertia moment analysis | Orientation matrix |
| | Dip direction |
| | S ₁ 271.36 |
| | S ₂ 60.13 |
| | S ₃ 171.59 |
| | Dip angle |
| | 57.79 |
| | 36.38 |
| | 74.92 |
| | Eigenvalue |
| | 0.861060 |
| | 0.087376 |
| | 0.051564 |

the expert. As a result, a two-dimensional cartographic model is produced that exhibits distinct orientation patterns. In the first variant ([Fig. 9A](#) and D) the observations genetically related to the fault are located within the central part of the chart. Using this partition, it is straightforward to recognize the fault. The next models revealed that naively establishing a narrow (10°) zone for the dip direction ([Fig. 9B](#) for vertical fault, [Fig. 9E](#) for fault dipping at 60°) led to underrepresentation of observations genetically related to fault. In this variant the fault was not recognized. A quasi-statistical approach is shown in [Fig. 9C](#) and F, where 90% directional variability intervals were established. Here the trajectory of the red points still served as the indicator of the fault but the limitation is that observations genetically related to the fault were assigned to a domain that is unrelated to the fault (blue on [Fig. 9](#)).

Table 5

Results from computing the orientation for the 60° dipping fault model: with triangulation and using a combinatorial model that created all possible planes.

| | |
|---------------------------------|-------------------------------|
| Observations from triangulation | Number of observations |
| | 21 |
| Circular mean | Dip Direction |
| | 264.82 |
| Combinatorial model | Number of observations |
| | 3241 |
| Circular mean | Dip Direction |
| | 264.86 |
| Observations from triangulation | Number of observations |
| | 21 |
| Inertia moment analysis | Orientation matrix |
| | Dip direction |
| | S ₁ 263.51 |
| | S ₂ 12.28 |
| | S ₃ 104.47 |
| | Dip angle |
| | 19.60 |
| | 83.46 |
| | 71.61 |
| | Eigenvalue |
| | 0.964710 |
| | 0.025634 |
| | 0.009657 |
| Combinatorial model | Number of observations |
| | 3241 |
| Inertia moment analysis | Orientation matrix |
| | Dip direction |
| | S ₁ 266.61 |
| | S ₂ 96.07 |
| | S ₃ 5.51 |
| | Dip angle |
| | 14.23 |
| | 75.95 |
| | 87.75 |
| | Eigenvalue |
| | 0.925493 |
| | 0.056275 |
| | 0.018232 |

6. Discussion

The main objective of this research was to investigate to what extent the *three-point approach* applied to triangulated surfaces is capable of calculating the orientation of faults. Ultimately, this study was intended to assess the ability of conducting spatial clustering on faulted geological surfaces using borehole data and triangulation. We considered two synthetic fault models: one with a vertically oriented fault and one dipping at 60°. The main difference between them is that the latter has the potential of broadening the zone grouping triangles that are genetically related to fault. This is because the boreholes may lie within the zone in which the fault plane itself separates the geological units. In our case study, we used a simplified model in which the geological contact surfaces were horizontal. This simplification allowed triangles that are

Table 6

Selected summary statistics: 90T and 90C – triangulated and combinatorial models for vertical faults, respectively; 60T and 60C – triangulated and combinatorial models for inclined fault, respectively.

| | 90T | 90C | 60T | 60C |
|---|------------------|------------------|------------------|------------------|
| Number of observations | 21 | 3150 | 21 | 3241 |
| Mean direction | 269.62 | 272.75 | 264.82 | 264.86 |
| Median direction | 272.20 | 271.53 | 262.88 | 267.79 |
| Resultant length | 16.95 | 2611.62 | 19.00 | 2641.18 |
| Mean resultant length | 0.81 | 0.83 | 0.90 | 0.81 |
| Circular standard deviation | 37.51 | 35.08 | 25.63 | 36.66 |
| Estimate of circular dispersion | 0.4793 | 0.1366 | 0.2056 | 0.1968 |
| Circular standard error | 0.1511 | 0.0066 | 0.0989 | 0.0078 |
| Von Mises concentration parameter estimate | 2.95 | 3.27 | 5.54 | 3.06 |
| 95% confidence intervals for mean direction | [262.78, 276.45] | [272.44, 273.07] | [253.80, 275.83] | [263.99, 265.74] |

genetically related to faults to be easily identified, which would have been more difficult to achieve if additional dip or stratigraphic noise were introduced. However, in general, the attitude of a triangle genetically related to a fault is only a proxy of the fault orientation because it is influenced by both the fault and contact surface geometry.

The proposed methodology is limited to better calculating the fault strike but not the dip direction. This observation follows from the fact that the distribution of dip direction associated with triangles genetically related to a fault can be essentially attributed to both normal and reverse faults underlying this distribution. But in a case of a reverse fault (Fig. 4C) the dip direction of the fault would be opposite to that of the triangles. Therefore, to obtain the fault strike, 90° should be added to the calculated mean dip direction for the triangles' population. Theoretically, the dip direction of triangles could be consistent with the dip direction of a reverse fault, but this would require repeated layers in a borehole. However, this effect is equivalent to identifying a reverse fault, and our method is offered if no preferential effects of this kind are available. Although we investigated the directional variability of triangles genetically related to faults, this approach may not be sufficient for identifying faults striking perpendicular to the preferred dip direction, which is the case for homoclines (Michalak et al., 2019). Thus, distinguishing such faults from the preferred dip direction should also involve an analysis of the dip angle. Another limitation is that this method would make no difference between a fault and a ramp, which is the case for en echelon structures (Julio et al., 2015a, 2015b).

Visual inspection of the synthetic models suggests that the triangles are more likely to have a direction similar to the true direction of the fault dip after applying the combinatorial algorithm. However, this effect may be due to a sampling bias in the sense that we investigated an elongated zone in which boreholes were distributed evenly along the fault strike. Currently, too little knowledge about the method is available to confirm or reject the sampling bias hypothesis. However, we suggest that new experiments should be performed with points distributed along a line that is oblique to the fault strike. The resulting orientation distribution should then be analyzed for the possibility of inferring the true dip direction. From a statistical viewpoint, the main difference between the triangulation-based and combinatorial results is related to the circular standard error (Table 6). While the values of circular dispersion are similar between models, they change significantly if they are divided by n (according to the formula for circular standard error), which is significantly greater for the combinatorial model. Using the combinatorial extension turned out to be also instructive in terms of showing the geometric singularities that otherwise could remain unnoticed. The number of counterintuitive orientations dipping in the eastern direction is relatively small, and the values

of the resultant length (Table 6) suggest that the resulting distribution can be considered unimodal (Mardia and Jupp, 2008). These effects are not negligible in the sense that both the directional correlations (the same dip directions for different triangles), as well as orientation singularities, may be controlled by a general geometric rule. We hypothesize that the dip direction of a triangle genetically related to a fault is controlled by the direction of the edge lying on the horizontal part (hanging wall or footwall) and the position of the third point relative to this edge, that is, whether it lies to the left or to the right side of this edge. Further research is needed to confirm or disprove this hypothesis, including the application of computational geometry theorems and formal proofs.

It should also be noted that we used the two-dimensional representation of the orientation data and the colorful points were assigned to geometric centers of the Delaunay triangles. Thus, conducting spatial clustering in our methodology was sensitive to, or biased by, the selection of the representative point from a triangle's interior. Considering more points from these interiors or the construction of regular grids could be thus a potential solution to the representativeness problem.

The inherent feature of the proposed methodology is that the map used for conducting spatial clustering depends on the initial partition of orientation measurements. While considering a narrow zone for the triangles' dip direction can ultimately lead to many undetected faults, establishing a wide interval on the other hand can lead to false positive results, i.e., recognition of faults that in reality do not exist. To address this issue, we therefore proposed a *quasi*-statistical approach to determine a reasonable directional variability interval. In this non-parametric method, establishing a directional variability interval for the directional data is however sensitive to the proper identification of outlying observations. A more statistically rigorous approach should be therefore developed, including parametric fitting of the models, and testing statistical hypotheses for mean directions or symmetry of the underlying distribution.

7. Conclusions

This study undertook an experiment based on applying a combinatorial algorithm to two sets of boreholes representing faulted surfaces. The proposed algorithm extended the set of observations genetically related to faults, which helped identify the potential strengths and limitations of the three-point method. While the epistemic objective was to obtain better knowledge about the fault strike, the results identified problems of further theoretical and experimental interest (Watson, 1966). Studying the conflict inherent to the combination of methods, that is, between reducing the epistemic uncertainty and releasing the observations from the triangulation-induced constructional constraints, resulted in the following conclusions:

- The three-point approach in a faulted area must be used with caution as it can give counterintuitive dip directions for triangles cutting a fault (Fig. 3F).
- Counterexamples were provided to justify that the proposed approach should not be used for the estimation of the lower bound on the fault dip (dip angles greater than 60 in Table 3).
- The method does not have the potential of indicating the fault dip direction but only the relative positions of hanging wall and footwall (see reverse faults, Fig. 4C).
- Although the orientations sampled throughout a triangulated surface are three-dimensional in nature, in the case of a faulted surface, the inclination aspect of these orientations does not seem to be of particular interest. Instead, the directional aspect can be used with reasonable success for conducting spatial clustering. The dip angles must be however analyzed if the hypothesized faults strike perpendicular to the preferred dip direction.
- The combinatorial algorithm of generating all three-element subsets from an n -element set may be used to better assess the directional

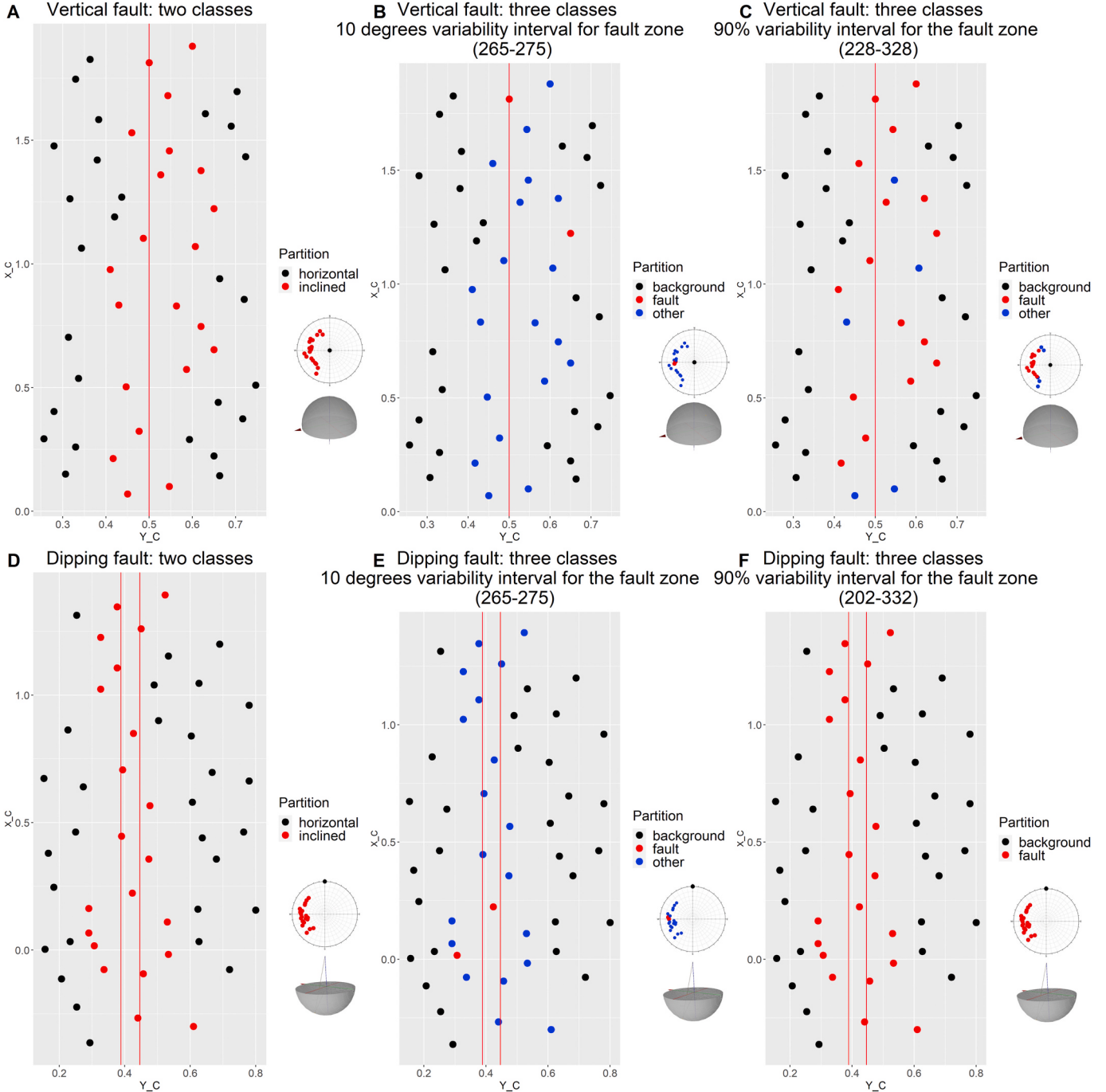


Fig. 9. The geometric centers of Delaunay triangles are color-coded with respect to the class with which they are associated based on an user-guided partition of orientations (A-C - normal vector representation with upper hemisphere; D-F - dip vector representation with lower hemisphere): (A) vertical fault with horizontal and inclined classes; (B) vertical fault with three classes with a narrow zone of 10° around the expected dip direction; (C) vertical fault with three classes corresponding to the 90% directional variability interval approach; (D) non-vertical fault with horizontal and inclined classes; (E) non-vertical fault with three classes with a narrow zone of 10° around the expected dip direction; (F) non-vertical fault with three classes corresponding to the 90% directional variability interval approach (please note that there are only two classes because the calculated 90% directional variability interval covered all observations genetically related to fault). (For interpretation of the references to color in this figure legend, the reader is referred to the Web version of this article.)

variability interval for the fault strike that can be further used for conducting spatial clustering.

- Three features of the resulting distributions were not explained and require further studies: 1) the same value of dip direction for different triangles; 2) concentration of triangles around the true dip direction; and 3) “counterintuitive” dip directions of triangles. We believe that these effects should be explained within the framework of computational geometry theorems and formal proofs.

- Compared to an identification obtained through automatic methods (e.g. cluster analysis), the main advantage of the method is that it allows the investigation of poorly represented orientations for indicating spatial patterns. This may be particularly useful for testing whether hypothesized structures are present within a region of interest.
- The patterns obtained through the proposed maps are clearly sensitive to the selection of the points representing a triangle. Taking

more points from its interior or making a regularized (grid) version could be a solution to this problem.

Computer code availability

Name of code: OCT, 3GeoCombine. **License:** GNU General Public License v3.0. **Developer:** Michał Michalak. **Contact address:** Institute of Earth Sciences, University of Silesia in Katowice, Poland. E-mail: mimichalak@us.edu.pl. **Year first available:** 2018 (OCT), 2019 (3GeoCombine). **Hardware required:** Celeron CPU or better. **Software required:** Microsoft Visual Studio (2015, 2017), ParaView (ver. 5.6.0). **Program language:** C++. **Program size:** 600 KB. **How to access the source code:** Available at: <https://github.com/michalmichalak997/OCT>, <https://github.com/michalmichalak997/3GeoCombine> (experimental branch).

Data Availability

Data input developed for the synthetic case studies as well as data output are open-source and freely accessible. Please visit: <https://github.com/michalmichalak997/3GeoCombine> (CaseStudies.zip and Case_Studies_Supplementary.zip files).

Declaration of competing interest

The authors declare that they have no known competing financial interests or personal relationships that could have appeared to influence the work reported in this paper.

Acknowledgements

Language-editing service was supported twice by the Faculty of Earth Sciences, University of Silesia in Katowice from a subsidy from the Polish Ministry of Science and Higher Education for research and development works. Three anonymous reviewers helped 1) achieve a greater balance between statistical and geometrical portions of the paper and also, 2) detect technical inaccuracies and 3) enhance the originality of the proposed approach. Gautier Laurent is thanked for his careful, insightful and constructive comments especially regarding unnoticed limitations and subjectivity that hopefully inspire future research in this field.

Appendix A. Supplementary data

Supplementary data to this article can be found online at <https://doi.org/10.1016/j.cageo.2021.104777>.

References

- Allmendinger, R.W., 2020. GMDE: extracting quantitative information from geologic maps. *Geosphere* 16, 1495–1507. <https://doi.org/10.1130/GES02253.1>.
- Bandpey, A.K., Shahriar, K., Sharifzadeh, M., Marezvand, P., 2019. Comparison of methods for calculating geometrical characteristics of discontinuities in a cavern of the Rudbar Lorestan power plant. *Bull. Eng. Geol. Environ.* 78, 1073–1093. <https://doi.org/10.1007/s10064-017-1145-x>.
- Boussouat, J.D., Devillers, O., Pion, S., Teillaud, M., Yvinec, M., 2002. Triangulations in CGAL. *Comput. Geom. Theory Appl.* 22, 5–19. [https://doi.org/10.1016/S0925-7721\(01\)00054-2](https://doi.org/10.1016/S0925-7721(01)00054-2).
- Bond, C.E., 2015. Uncertainty in structural interpretation: lessons to be learnt. *J. Struct. Geol.* 74, 185–200. <https://doi.org/10.1016/j.jsg.2015.03.003>.
- Bond, C.E., Gibbs, A.D., Shipton, Z.K., Jones, S., 2007a. What do you think this is? “Conceptual uncertainty” in geoscience interpretation. *GSA Today (Geol. Soc. Am.)* 17, 4–10. <https://doi.org/10.1130/GSAT01711A.1>.
- Bond, C.E., Shipton, Z.K., Jones, R.R., Butler, R.W.H., Gibbs, A.D., 2007b. Knowledge transfer in a digital world: field data acquisition, uncertainty, Visualization, and data management. *Geosphere* 3, 568–576. <https://doi.org/10.1130/GES00094.1>.
- Brideau, M.A., Sturzenegger, M., Stead, D., Jaboyedoff, M., Lawrence, M., Roberts, N., Ward, B., Millard, T., Clague, J., 2012. Stability analysis of the 2007 Chehalis lake landslide based on long-range terrestrial photogrammetry and airborne LiDAR data. *Landslides* 9, 75–91. <https://doi.org/10.1007/s10346-011-0286-4>.
- Bruna, P.O., Straubhaar, J., Prabhakaran, R., Bertotti, G., Bisdom, K., Mariethoz, G., Meda, M., 2019. A new methodology to train fracture network simulation using multiple-point statistics. *Solid Earth* 10, 537–559. <https://doi.org/10.5194/se-10-537-2019>.
- Caumon, G., Collon-Drouaillet, P., Le Carlier De Veslud, C., Viseur, S., Sausse, J., 2009. Surface-based 3D modeling of geological structures. *Math. Geosci.* 41, 927–945. <https://doi.org/10.1007/s11004-009-9244-2>.
- CGAL.org, n.d. Cgal, Computational Geometry Algorithms Library.
- Chen, J., Zhu, H., Li, X., 2016. Automatic extraction of discontinuity orientation from rock mass surface 3D point cloud. *Comput. Geosci.* 95, 18–31. <https://doi.org/10.1016/j.cageo.2016.06.015>.
- Childs, C., Manzocchi, T., Walsh, J.J., Bonson, C.G., Nicol, A., Schöpfer, M.P.J., 2009. A geometric model of fault zone and fault rock thickness variations. *J. Struct. Geol.* 31, 117–127. <https://doi.org/10.1016/j.jsg.2008.08.009>.
- Collon, P., Steckiewicz-Laurent, W., Pellerin, J., Laurent, G., Caumon, G., Reichart, G., Vaute, L., 2015. 3D geomodelling combining implicit surfaces and Voronoi-based remeshing: a case study in the Lorraine Coal Basin (France). *Comput. Geosci.* 77, 29–43. <https://doi.org/10.1016/j.cageo.2015.01.009>.
- Coubal, M., Adamović, J., Málek, J., Prouza, V., 2014. Architecture of thrust faults with alongstrike variations in fault-plane dip: anatomy of the Lusatian fault, Bohemian Massif. *J. Geosci.* 59, 183–208. <https://doi.org/10.3190/jgeosci.174>.
- Davis, J.C., 2002. *Statistics and Data Analysis in Geology*, third ed. Wiley, New York.
- De Berg, M., Cheong, O., Van Kreveld, M., Overmars, M., 2008. *Computational Geometry: Algorithms and Applications*, Computational Geometry. <https://doi.org/10.2307/3620533>.
- Dewez, T.J.B., Girardeau-Montaut, D., Allanic, C., Rohmer, J., 2016. Facets: a cloudcompare plugin to extract geological planes from unstructured 3d point clouds. In: International Archives of the Photogrammetry, Remote Sensing and Spatial Information Sciences - ISPRS Archives, pp. 799–804. <https://doi.org/10.5194/isprarchives-XLI-B5-799-2016>.
- Drews, T., Miernik, G., Anders, K., Höfle, B., Profe, J., Emmerich, A., Bechstädt, T., 2018. Validation of fracture data recognition in rock masses by automated plane detection in 3D point clouds. *Int. J. Rock Mech. Min. Sci.* 109, 19–31. <https://doi.org/10.1016/j.ijrmms.2018.06.023>.
- Fara, H., Scheidegger, A., 1961. Statistical geometry of porous media. *J. Geophys. Res.* 66, 3279–3284.
- Ferrero, A.M., Forlani, G., Roncella, R., Voyat, H.I., 2009. Advanced geostructural survey methods applied to rock mass characterization. *Rock Mech. Rock Eng.* 42, 631–665. <https://doi.org/10.1007/s00603-008-0010-4>.
- Fisher, N.I., 1993. *Statistical Analysis of Circular Data*. Cambridge University Press. <https://doi.org/10.1017/cbo9780511564345>.
- Fisher, N.I., Huntingdon, J.F., Jacket, D.R., Willcox, M.E., Creasey, J.W., 1985. Spatial analysis of two-dimensional orientation data. *J. Int. Assoc. Math. Geol.* 17, 177–194. <https://doi.org/10.1007/BF01033153>.
- Fisher, N.I., Lewis, T., Embleton, B.J.J., 1993. Statistical analysis of spherical data. *Stat. Anal. spherical data* 329pp. <https://doi.org/10.2307/3620138>.
- Gallo, L.C., Cristallini, E.O., Svarc, M., 2018. A nonparametric approach for assessing precision in georeferenced point clouds best fit planes: toward more reliable thresholds. *J. Geophys. Res. Solid Earth* 123, 10297–10308. <https://doi.org/10.1029/2018JB016319>.
- Ge, Y., Tang, H., Xia, D., Wang, L., Zhao, B., Teaway, J.W., Chen, H., Zhou, T., 2018. Automated measurements of discontinuity geometric properties from a 3D-point cloud based on a modified region growing algorithm. *Eng. Geol.* 242, 44–54. <https://doi.org/10.1016/j.enggeo.2018.05.007>.
- Gigli, G., Casagli, N., 2011. Semi-automatic extraction of rock mass structural data from high resolution LIDAR point clouds. *Int. J. Rock Mech. Min. Sci.* 48, 187–198. <https://doi.org/10.1016/j.ijrmms.2010.11.009>.
- Godefroy, G., Caumon, G., Laurent, G., Bonneau, F., 2021. Multi-scenario interpretations from sparse fault evidence using graph theory and geological rules. *J. Geophys. Res. Solid Earth* 126, e2020JB020022. <https://doi.org/10.1029/2020JB020022>.
- Godefroy, G., Caumon, G., Laurent, G., Bonneau, F., 2019. Structural interpretation of sparse fault data using graph theory and geological rules: fault data interpretation. *Math. Geosci.* 51, 1091–1107. <https://doi.org/10.1007/s11004-019-09800-0>.
- Goldberg, D., 1991. What every computer scientist should know about floating-point arithmetic. *ACM Comput. Surv.* 23, 5–48. <https://doi.org/10.1145/103162.103163>.
- Gomes, R.K., De Oliveira, L.P.L., Gonzaga, L., Tognoli, F.M.W., Veronez, M.R., De Souza, M.K., 2016. An algorithm for automatic detection and orientation estimation of planar structures in LiDAR-scanned outcrops. *Comput. Geosci.* 90, 170–178. <https://doi.org/10.1016/j.cageo.2016.02.011>.
- Gonçalves, I.G., Guadagnin, F., Kumaira, S., Da Silva, S.L., 2021. A machine learning model for structural trend fields. *Comput. Geosci.* 149, 104715. <https://doi.org/10.1016/j.cageo.2021.104715>.
- Górecka, E., 2013. Geological setting of the Silesian-Cracow Zn-Pb deposits. *Geol. Q.* 57, 127–146.
- Groshong, R.H., 2006. 3-D Structural Geology, 3-D Structural Geology: A Practical Guide to Quantitative Surface and Subsurface Map Interpretation. <https://doi.org/10.1007/978-3-540-31055-6>.
- Guo, J., Liu, Y., Wu, L., Liu, S., Yang, T., Zhu, W., Zhang, Z., 2019. A geometry- and texture-based automatic discontinuity trace extraction method for rock mass point cloud. *Int. J. Rock Mech. Min. Sci.* 124, 104132. <https://doi.org/10.1016/j.ijrmms.2019.104132>.
- Jones, R.R., Pearce, M.A., Jacquemyn, C., Watson, F.E., 2016. Robust best-fit planes from geospatial data. *Geosphere* 12, 196–202. <https://doi.org/10.1130/GES01247.1>.
- Julio, C., Caumon, G., Ford, M., 2015a. Impact of the en echelon fault connectivity on reservoir flow simulations. *Interpretation* 3, SAC23–SAC34. <https://doi.org/10.1190/INT-2015-0060.1>.

- Julio, C., Caumon, G., Ford, M., 2015b. Sampling the uncertainty associated with segmented normal fault interpretation using a stochastic downscaling method. *Tectonophysics* 639, 56–67. <https://doi.org/10.1016/j.tecto.2014.11.013>.
- Kiureghian, A., Der, Ditlevsen, O., 2009. Aleatory or epistemic? Does it matter? *Struct. Saf.* 31, 105–112. <https://doi.org/10.1016/j.strusafe.2008.06.020>.
- Lato, M., Diederichs, M.S., Hutchinson, D.J., Harrap, R., 2009. Optimization of LiDAR scanning and processing for automated structural evaluation of discontinuities in rockmasses. *Int. J. Rock Mech. Min. Sci.* 46, 194–199. <https://doi.org/10.1016/j.ijrmms.2008.04.007>.
- Lato, M.J., Diederichs, M.S., Hutchinson, D.J., Harrap, R., 2012. Evaluating roadside rockmasses for rockfall hazards using LiDAR data: optimizing data collection and processing protocols. *Nat. Hazards* 60, 831–864. <https://doi.org/10.1007/s11069-011-9872-y>.
- Lipski, W., 2004. *Combinatorics for Programmers*. Wydawnictwa Naukowo-Techniczne, Warszawa.
- MacCormack, K., Arnaud, E., Parker, B.L., 2018. Using a multiple variogram approach to improve the accuracy of subsurface geological models. *Can. J. Earth Sci.* 55, 786–801. <https://doi.org/10.1139/cjes-2016-0112>.
- Maerz, N.H., Youssef, A.M., Otoo, J.N., Kassebaum, T.J., Duan, Y., 2013. A simple method for measuring discontinuity orientations from terrestrial LIDAR data. *Environ. Eng. Geosci.* 19, 185–194. <https://doi.org/10.2113/gsgeosci.19.2.185>.
- Mardia, K.V., Jupp, P.E., 2008. *Directional Statistics*. Wiley. <https://doi.org/10.1002/9780470316979>.
- Marynowski, L., Zatoń, M., Simoneit, B., Otto, A., Jędrysek, M.O., Grelowski, C., Kurkiewicz, S., 2007. Compositions, sources and depositional environments of organic matter from the Middle Jurassic clays of Poland. *Appl. Geochem.* 22, 2456–2485. <https://doi.org/10.1016/j.apgeochem.2007.06.015>.
- Matasci, B., Stock, G.M., Jaboyedoff, M., Carrea, D., Collins, B.D., Guérin, A., Matasci, G., Ravanel, L., 2018. Assessing rockfall susceptibility in steep and overhanging slopes using three-dimensional analysis of failure mechanisms. *Landslides* 15, 859–878. <https://doi.org/10.1007/s10346-017-0911-y>.
- Michałak, M., 2018. Numerical limitations of the attainment of the orientation of geological planes. *Open Geosci.* 10 <https://doi.org/10.1515/geo-2018-0031>.
- Michałak, M.P., Bardziński, W., Teper, L., Małolepszy, Z., 2019. Using Delaunay triangulation and cluster analysis to determine the orientation of a sub-horizontal and noisy including contact in Kraków-Silesian Homocline, Poland. *Comput. Geosci.* 133, 104322. <https://doi.org/10.1016/j.cageo.2019.104322>.
- Pakyuz-Charrier, E., Lindsay, M., Ogarko, V., Giraud, J., Jessell, M., 2018. Monte Carlo simulation for uncertainty estimation on structural data in implicit 3-D geological modeling, a guide for disturbance distribution selection and parameterization. *Solid Earth* 9, 385–402. <https://doi.org/10.5194/se-9-385-2018>.
- Riquelme, A.J., Abellán, A., Tomás, R., Jaboyedoff, M., 2014. A new approach for semi-automatic rock mass joints recognition from 3D point clouds. *Comput. Geosci.* 68, 38–52. <https://doi.org/10.1016/j.cageo.2014.03.014>.
- Scheidegger, A.E., 1965a. The tectonic stress and tectonic motion direction in the Pacific and adjacent areas as calculated from earthquake fault plane solutions. *Bull. Seismol. Soc. Am.* 55, 147–152.
- Scheidegger, A.E., 1965b. On the statistics of the orientation of bedding planes, grain axes, and similar sedimentological data. *U. S. Geol. Surv. Prof. Pap.* 525, 164–167.
- Schneeberger, R., De La Varga, M., Egli, D., Berger, A., Kober, F., Wellmann, F., Herwegh, M., 2017. Methods and uncertainty estimations of 3-D structural modelling in crystalline rocks: a case study. *Solid Earth* 8, 987–1002. <https://doi.org/10.5194/se-8-987-2017>.
- Seers, T.D., Hodgetts, D., 2016. Probabilistic constraints on structural lineament best fit plane precision obtained through numerical analysis. *J. Struct. Geol.* 82, 37–47. <https://doi.org/10.1016/j.jsg.2015.11.004>.
- Thiele, S.T., Jessell, M.W., Lindsay, M., Ogarko, V., Wellmann, J.F., Pakyuz-Charrier, E., 2016. The topology of geology 1: topological analysis. *J. Struct. Geol.* 91, 27–38. <https://doi.org/10.1016/j.jsg.2016.08.009>.
- Umili, G., Ferrero, A., Einstein, H.H., 2013. A new method for automatic discontinuity traces sampling on rock mass 3D model. *Comput. Geosci.* 51, 182–192. <https://doi.org/10.1016/j.cageo.2012.07.026>.
- Wang, X., Zou, L., Shen, X., Ren, Y., Qin, Y., 2017. A region-growing approach for automatic outcrop fracture extraction from a three-dimensional point cloud. *Comput. Geosci.* 99, 100–106. <https://doi.org/10.1016/j.cageo.2016.11.002>.
- Watson, G., 1965. Equatorial distributions on a sphere. *Biometrika* 52, 193–201. <https://doi.org/10.1093/biomet/52.1.2.193>.
- Watson, G.S., 1966. The statistics of orientation data. *J. Geol.* 74, 786–797. <https://doi.org/10.1086/627211>.
- Wellmann, F.J., Horowitz, F.G., Schill, E., Regenauer-Lieb, K., 2010. Towards incorporating uncertainty of structural data in 3D geological inversion. *Tectonophysics* 490, 141–151. <https://doi.org/10.1016/j.tecto.2010.04.022>.
- Wellmann, F.J., Thiele, S.T., Lindsay, M.D., Jessell, M.W., 2016. Pynoddy 1.0: an experimental platform for automated 3-D kinematic and potential field modelling. *Geosci. Model Dev. (GMD)* 8, 10011–10051. <https://doi.org/10.5194/gmd-9-1019-2016>.
- Woodcock, N.H., 1977. Specification of fabric shapes using an eigenvalue method. *Bull. Geol. Soc. Am.* 88, 1231–1236. [https://doi.org/10.1130/0016-7606\(1977\)88<1231:SOFSUA>2.0.CO;2](https://doi.org/10.1130/0016-7606(1977)88<1231:SOFSUA>2.0.CO;2).
- Woźniak, T., Bania, G., 2019. Analysis of the tectonic and sedimentary features of the southern margin of the Krzeszowice Graben in Southern Poland based on an integrated geoelectrical and geological studies. *J. Appl. Geophys.* 165, 60–76. <https://doi.org/10.1016/j.jappgeo.2019.04.010>.
- Woźniak, T., Bania, G., Mościcki, W.J., Ćwiklik, M., 2018. Electrical resistivity tomography (ERT) and sedimentological analysis applied to investigation of upper Jurassic limestones from the Krzeszowice Graben (Kraków Upland, southern Poland). *Geol. Q.* 62, 287–302. <https://doi.org/10.7306/gq.1403>.
- Wu, X., Zhu, Z., 2017. Methods to enhance seismic faults and construct fault surfaces. *Comput. Geosci.* 107, 37–48. <https://doi.org/10.1016/j.cageo.2017.06.015>.
- Znosko, J., 1960. *Tektonika obszaru częstochowskiego*. *Przegląd Geol.* 8, 418–424.